JOURNAL OF AIRCRAFT
Vol. 37, No. 1, January–February 2000

Linking Riveting Process Parameters to the Fatigue Performance of Riveted Aircraft Structures

M. P. Szolwinski*
Rensselaer Polytechnic Institute, Troy, New York 12180-3590
and
T. N. Farris†
Purdue University, West Lafayette, Indiana 47907-1282

The onset of widespread fatigue damage in riveted aircraft structure has been linked to sharp gradients of stress arising from contact between rivets and rivet holes. In addition, the mechanics of load transfer in lap joint structure (and resulting damage) is influenced by the through-thickness restraint offered by the installed rivet. Finally, the propagation of fatigue cracks at and around the rivet/hole interface is tied to the residual stress field induced during the riveting process. In light of the influence that rivet installation has on the fatigue performance of riveted joints, the aim was to link details of a quasi-static, squeeze force-controlled riveting process as provided by finite element modeling to the resulting residual stress field in a single-lap joint structure. Supporting experiments provide insight into the inelastic response of the rivet material and validation of the model results. These results from the model reveal both a strong through-thickness gradient in residual stresses and a change in the distribution of residual hoop stress near the rivet/hole interface with squeeze force. Comments are also made regarding the relationship between riveting process parameters and trends in observed fatigue failures of riveted lap joint test articles.

Introduction

IN the two decades following the official adoption of the damage tolerant approach, advances in the understanding of basic fatigue mechanisms, damage tolerant structural design, nondestructive inspection techniques and a comprehensive tracking of individual aircraft usage have provided the U.S. Air Force with confidence in this philosophy of ensuring the structural integrity of its fleet. However, successful, robust, and cost-effective implementation of the damage tolerant approach hinges on two elements: the capability to inspect critical structural elements and the ability to blend predictive tools with laboratory and operational service data to schedule appropriate inspection intervals. The aftermath of the 1988 Aloha Airlines flight 243 incident, in which a portion of the passenger compartment disintegrated during a short flight, forced the aerospace community to refocus the procedure developed to ensure the structural integrity of aircraft, civilian and military alike.

Expert review of the watershed Aloha Airlines incident attributed the disaster to the sudden linking of multiple undetected cracks at and around rivet holes in the metallic panels comprising the skin of the pressurized fuselage. This in-flight catastrophe unveiled the potential threat to airframe structural integrity proffered by the interaction and uncontrolled linkup of seemingly small and often undetectable cracks in riveted primary structure. This type of fatigue damage, often referred to as widespread fatigue damage (WFD), is characteristic of the large population of aging aircraft. WFD poses a current dual-tiered threat to the basis of the damage tolerant design philosophy because 1) it often defies detection by pragmatic nondestructive inspection of riveted structure and 2) the knowledge base on the nucleation of this type of damage is only beginning to mature. Consequently, a critical need exists currently to identify and understand the detailed relationship between the factors that control the development of WFD and the subsequent fatigue performance of riveted aircraft components.

Motivated by observations from both periodic teardown inspections of aging aircraft structure and laboratory tests of riveted lap splice joint configurations,[1–4] this research was targeted at developing an accurate understanding of the localized conditions at and around the rivet/hole interface introduced during rivet installation. To this end, a finite element model of a force-controlled rivet installation process was formulated with an experimental characterization of the inelastic material response associated with the large-scale deformation of the rivet material. Verification of this formulation relied on validation of the large- and small-scale plastic deformation associated with the forming of the driven rivet head and hole expansion.

Results from several analyses are then interpreted in the context of the mechanics of load transfer in riveted joints and the intimately related nucleation and propagation of fatigue damage, including fretting fatigue cracks, in riveted lap joint test articles. Final comments are made regarding juxtaposition of this analysis tool with a global joint model to establish design-based criteria for the manufacturing and subsequent fatigue performance of riveted aircraft structure.

Motivation

Typical riveted aircraft structure is manufactured by layering either two (single-lap joint) or three (double-lap joint) sheets of material and then joining the assembly together with a fastener. Common fastening techniques rely on either bolts or other threaded fasteners and rivets. When compared to threaded fasteners, the use of rivets is more attractive because of both its economical advantages (no threading of bulk material required, lower unit cost for the fastener, and faster cycle time for installation) and its permanence after installation (no ability to back out after installation). Figure 1 introduces the key features and vocabulary of rivet installation, including the expansion of the rivet shank against the surface of the drilled hole and the related forming or upsetting of a driven rivet head. This forming or heading process is referred to as bucking and is accomplished usually by impacting a tool against the manufactured rivet head while providing resistance against the driven rivet head with a flat bucking bar surface. The tool can be driven by hydraulic, pneumatic, electro-magnetic, or manual actuation.

Received 18 February 1999; presented as Paper 99-1339 at the AIAA/ASME/ASCE/AHS/ASC 40th Structures, Structural Dynamics, and Materials Conference, St. Louis, MO, 12–15 April 1999; revision received 30 June 1999; accepted for publication 10 July 1999.

*Assistant Professor, Department of Mechanical Engineering, Aeronautical Engineering and Mechanics. Member AIAA.

†Professor and Head, School of Aeronautics and Astronautics. Associate Fellow AIAA.

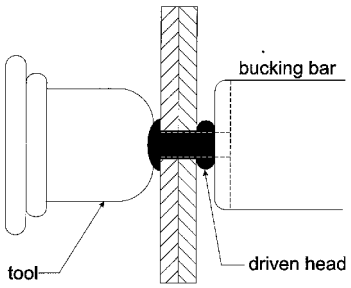

Fig. 1 Summary of the key features and nomenclature of rivet installation (adapted from an illustration by Reithmaier).[17]

The bulk of published research on riveted joints, including work by Beuth and Hutchinson[5] and Park and Alturi,[6] provides little insight into either the link between the rivet installation process and the resulting contact conditions, or the subsequent interaction between the installed rivet and surrounding material during loading of the manufactured joint. Most workers have avoided a detailed analysis of these contact conditions by accounting for the complex interaction between rivet and sheet by either introducing an artificial interference condition between a rigid pin and the rivet hole or simply calculating the resulting radial residual stresses due to uniform expansion of the rivet hole. Even for models that attempted to resolve the contact in more detail, uniform interference along the rivet and hole is assumed, and relatively unsubstantiated estimates of through-thickness clamping constraint provided by the installed rivets are used in the analyses.[7,8]

The need to understand more accurately the initial interference induced by rivet installation and the resulting residual stress field around the periphery of the hole is an obvious one. The nature of this residual stress field can have a profound impact on the nucleation and subsequent propagation of fatigue cracks emanating from near the edges of the hole. Treatments of the interference between the rivet and hole that neglect the high compressive stresses through the thickness direction during installation of the rivet cannot hope to capture the inelastic material response of both the rivet and surrounding sheet material.

Perhaps less obvious, though, is the influence of the clamping constraint provided through the thickness of the joint by the installed rivet heads on the potential for fretting damage at the faying surface. Results from a three-dimensional finite element model of a riveted joint by Harish and Farris illuminate this influence by emphasizing a dual mechanism of load transfer in a typical riveted lap joint configuration.[9] As presented schematically in Fig. 2, transfer of the applied bulk load through the joint is shared between frictional action at the faying surface and contact between the hole and plate. Although the model did not include the effects of interference between the rivet and hole, a qualitative understanding of the load transfer mechanism can be gleaned from its results.

Upon initial application of load to the joint with a slip fit rivet, the load is transferred solely through the frictional tractions at the interfacial or faying surface. As the load increases, the plates slip with respect to each other, bringing the rivet and hole into contact. (Note that it is this stick/slip behavior at the faying surfaces that leads to fretting damage in riveted lap joints.) Thus, increases in clamping constraint result in more frictional load transfer at the faying surfaces, whereas decreases in clamping pressure cause an increased loading at the interface between the rivet and hole periphery.

A fundamental question to those designing and manufacturing riveted aircraft structure centers on which of these conditions results in longer fatigue lifetimes. Should fastening techniques or installation methods that yield increased clamping constraint be employed, such that a larger percentage of the applied bulk load is transferred at the faying surface? Or will the increased severity of the fretting conditions at the faying surface result in more aggressive nucleation of fatigue damage away from the rivet hole?

Only a few researchers have attempted to answer this question systematically in research available in the archival literature.[2,10] One set of workers performed an exhaustive set of nearly 150 fatigue tests on 2024-T3 aluminum single-lap joint structures, subjected

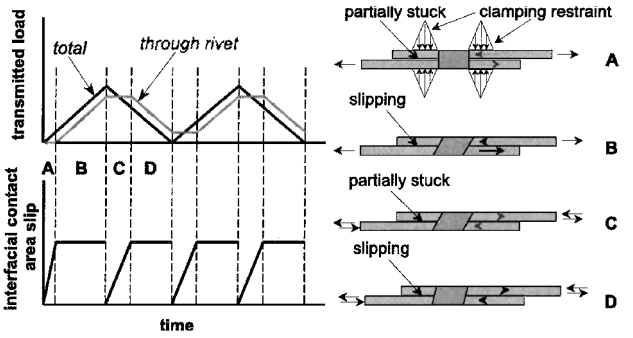

Fig. 2a Graphical representation of the dual load-transfer mechanism in a riveted lap joint, as derived from finite element results by Harish and Farris.[9]

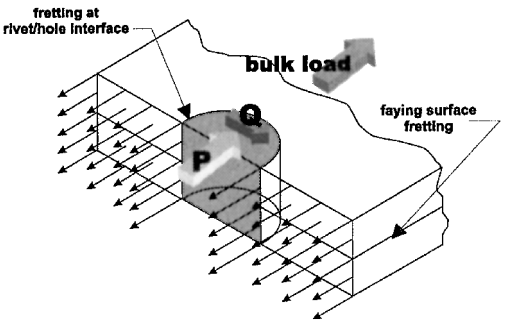

Fig. 2b Highlight of the critical regions for the nucleation of widespread fatigue damage by fretting at and around the rivet/hole interface in riveted aircraft structure.

to both constant-amplitude and spectrum loading representative of those experienced during aircraft service. The joints were assembled with a variety of techniques, including hydraulic, pneumatic, and hand riveting. In analyzing the results of fatigue tests, the researchers uncovered a correlation between a larger driven head size and increases in fatigue lifetime.

Müller also supported this observation in a well-constructed study of riveted lap joint structure.[2] To control the consistency of the conditions at and around the rivet/hole interface, this work validated a method of force-controlled rivet installation. In this approach, compressing the rivet/joint assembly quasi-statically between a set of hydraulic platens formed the rivet head. Unlike traditional impact riveting processes, where little control over the displacement of the tools is available, the force-controlled installation allows for precise control of the installation. Donaldson and Kenworthy have also reported increases in fatigue lives of joints assembled with this technique.[11] It is this squeeze-force technique that will be analyzed in the remainder of this paper.

Finite Element Model of Riveting

To assess the effects of rivet installation on the subsequent load transfer mechanics and related fatigue performance of riveted lap joints, a finite element model of force-controlled rivet installation was formulated. The objectives of the ensuing analysis were to quantify parametrically the effects of both squeeze force and material properties of the rivet and the surrounding sheet on the interference at the rivet/hole interface and residual stress field in the assembled joint. The configuration chosen for the modeling effort was composed of a standard 2117-T4 aluminum alloy universal head rivet (U.S. MILSPEC MS2047AD6-6, 0.1875 in. diam) and two 0.09-in. thick, bare 2024-T3 aluminum alloy plates. Review of the literature suggests that Müller was the first to report work of finite element modeling of rivet installation.[2] The work, though, models a symmetric slug rivet and countersink configuration. More importantly, the effort provides only limited results on the effects of material properties and the full residual stress field at and around the hole.

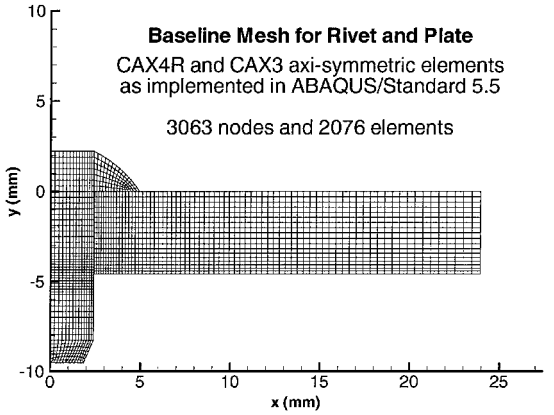

Fig. 3 Axisymmetric baseline mesh used in the finite element modeling of the rivet installation process.

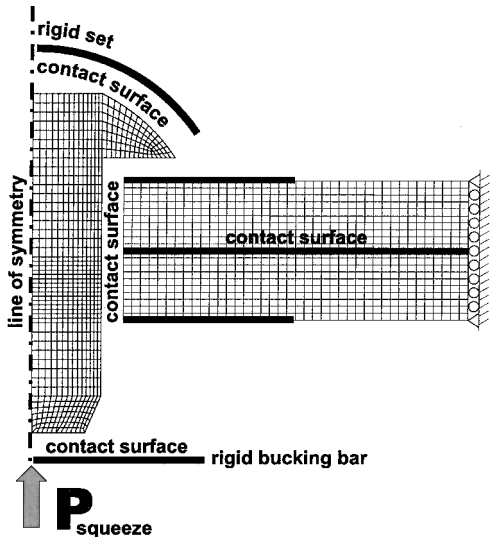

Fig. 4 Schematic of the finite element mesh of the tool/workpiece system; contact at the rivet/plate, plate/plate and rivet/tool interfaces are modeled.

A typical mesh and a schematic of the axisymmetric model are presented in Figs. 3 and 4, respectively. Macrofiles written in the command language for the software package MSC/PATRAN5 were used as a preprocessor for parametric generation of the mesh and associated input file for the computational engine chosen for the analysis, ABAQUS/Standard 5.5. Four-noded, axisymmetric elements with reduced integration (CAX4R) were employed to represent both the rivet and plates, with fewer than five triangular elements (CAX3) interspersed in the mesh. The mesh of the plates extended 10 rivet radii from the axis of symmetry, with rollers along these edge surfaces and a single edge node on each plate constrained in the y-direction to prevent rigid body modes. For a baseline mesh of approximately 2000 elements and 3000 nodes, runs were completed in under 3 h real time on a Sun Microsystems Ultra2 workstation with 512 MB of RAM.

As noted in Fig. 4, the model included contact both between the rivet and plates and at the faying surface or interface between the two plates. Also incorporated was the contact between the riveting tools, a fixed upper curved set and flat bucking surface, and the rivet. These tools were approximated in the model as rigid surfaces with no rotational degree of freedom. The contact analysis was conducted using the generalized contact pair approach with finite sliding option offered by ABAQUS. By employing this approach, no explicit definition of point-to-point contact elements was required; the user must only define pairs of master and slave surfaces, allowing ABAQUS to generate internal contact elements as needed to resolve the contact between each of the defined paired surfaces. A coefficient of friction of 0.20 was prescribed between all of the contact surfaces, reflecting data from friction tests with 2024-T351 aluminum alloy conducted in a separate study by Szolwinski.[12]

With details of the mesh and contact surfaces set, attention was given to the nature of the large-strain, elastic–plastic deformation present during the upsetting of the driven rivet head, deformation behavior present in many metal cutting and metal forming processes. In modeling this behavior successfully with the finite element method, two main concerns arose: 1) updating the finite element stiffness equations that depend on the current mesh geometry and state variables and 2) characterizing the nonlinear material behavior after exceeding initial yield, particularly for large strain values. In dealing with geometric nonlinearity, ABAQUS/Standard provided a nonlinear geometry option (NLGEOM) that formulates the elemental stiffnesses based on current configurations from deformed nodal positions. Because no small displacement assumptions are made, calculated stresses are then true stresses based on the deformed elemental configuration.[13]

Material Modeling

Inclusion of the nonlinear material behavior into the finite element model was a more tenuous task. Although copious amounts of monotonic tensile and compressive stress-strain data exists for 2024-T3 plate, surprisingly little data are present in the open literature for the rivet material, 2117-T4 (Ref. 14). In fact, the military standard for riveted joints specifies little about material properties of rivets, only mandating the installed shear strength of the rivet. Although a value for initial tensile yield strength for the alloy (24 ksi) was readily available, an absence of data for large-strain yielding behavior in compression, so critical for characterizing the upsetting of the driven head and the expansion of the rivet into the drilled hole, was noted.[15]

To estimate rivet-hardening properties for the model, a series of compression tests on billet samples extracted from 2117-T4 rivet shanks were conducted. Complete details of the test procedure can be found elsewhere.[12] As noted by Thomsen et al.,[16] static compression test data are often presented in the form $\sigma_{\text{true}} = C(\epsilon_{\text{true}})^m$ for a limited range of strain. Analysis of the force-deflection data from the compression tests yielded a value of $C = 79$ ksi (544 MPa) and $m = 0.23$ for the range of effective strain $0.02 \leq \epsilon_{\text{true}} \leq 0.10$.

Model Verification

To verify the model, including the choice of hardening parameters beyond the range of strain achieved in the compression tests, a series of 2024-T3 panels were riveted using a force-controlled setup and specimen design shown in Fig. 5. The rectangular grid pattern of 24

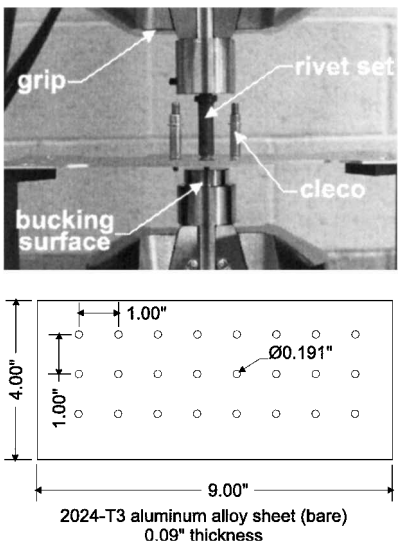

Fig. 5 Photograph of the force-controlled riveting setup and specimen design used in the verification of the finite element model.

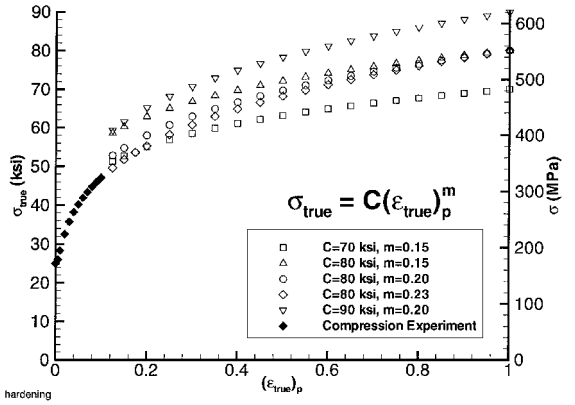

Fig. 6 Summary of the various compressive hardening behaviors considered in the series of trade studies comparing experimental and numerical force-deflection response during the riveting process.

holes with 1-in. spacing was produced with a computer numerical controlled vertical-machining center. Each of the holes was first located with a center drill pass, which was followed by a conventional drilling pass with a 0.1875-in. bit and a final pass with a number 11 reamer (0.191 in.). This procedure reflected practices suggested in a common aircraft industry handbook.[17] A mean radius of 0.0959 in. (standard deviation of 0.0003 in.) was determined from optical comparator measurements of 172 holes.

The force-controlled rivet installation was performed also with a computer-controlled 22 kip servohydraulic load frame equipped with grip fixturing to accommodate a curved rivet set in the top grip and a flat, polished bucking surface on the lower actuator. After initial contact was made between the bucking surface and the driven end of the rivet, the load was ramped quasi-statically (over a period of several seconds) to the target squeeze force. Six squeeze forces were considered in the current investigation: 2500, 3000, 3500, 4000, 4250, and 5000 lbf (11.1, 13.4, 15.6, 17.9, 19.0, and 22.4 kN, respectively).

Two sets of data were collected from these series of experiments for purposes of model verification. First, both applied force and bucking bar displacement were tracked and recorded during the riveting process, identical to the data collected during the compression tests. However, these data allowed for direct comparison with the force history and displacement response of the rigid bucking surface in the finite element model, a comparison used to determine the appropriate set of rivet material hardening parameters.

To this end, a series of numerical trade studies involving the baseline mesh were performed with a range of hardening parameters, as presented in Fig. 6. The hardening behavior was implemented in the model by providing a tabular listing of the points on the plot, with ABAQUS using linear interpolation for values between the points. Isotropic hardening was assumed for both the rivet and plate material.

As shown in Fig. 6, for compressive strains under 10%, the parameters generated from the compression tests of the billets of rivet material were used. To determine an appropriate material model beyond this range of strain, Fig. 7, which compares both experimental and numerical force-deflection histories of the interface between the tool (bucking bar) and workpiece (driven rivet head) was used. Based on these results, values of $C = 80$ ksi (551 MPa) and $m = 0.15$ were chosen. This choice is supported further by the excellent numerical agreement with experimental data generated at higher squeeze forces (see Fig. 8). A complete summary of the material properties used in the subsequent analyses is provided in Table 1.

In further validating the model, three rivet/hole locations were selected randomly and extracted carefully from the plates after rivet installation. Each of these samples was then sectioned near the symmetry plane of the rivet with a diamond saw and mounted in a bakelite disk. A series of fine polishing and measurement steps of the cross section followed, as suggested by Müller, to obtain the dimensions of the rivet/plate assembly at its plane of symmetry.[2]

Table 1 Summary of the elastic and plastic properties used for both the plate and rivet material

Parameter	Value
Young's modulus of plate	10.5×10^6 psi (72.4 GPa)
Poisson's ratio of plate	0.33
Initial yield stress for plate	40 ksi (276 MPa)
Slope of linear hardening curve for plate	2.5
Young's modulus of rivet material	10.4×10^6 psi (71.7 GPa)
Poisson's ratio of rivet material	0.33
Initial yield stress for rivet	24 ksi (172 MPa)
Hardening parameters for rivet, $0.02 \leq \epsilon_{\text{true}} \leq 0.10$	C = 79 ksi (544 MPa), m = 0.23
Hardening parameters for rivet, $0.10 < \epsilon_{\text{true}} \leq 1.0$	C = 80 ksi (551 MPa), m = 0.15

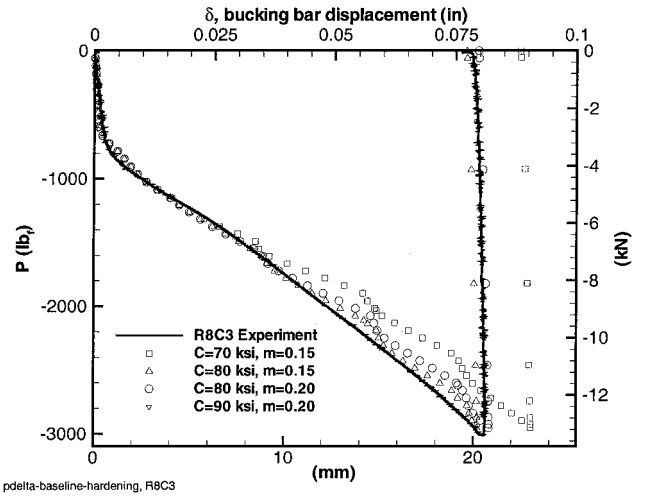

Fig. 7 Experimental force-deflection history, with $P_{\max}$ = 3000 lbf (13.4 kN), compared with results from the finite element model.

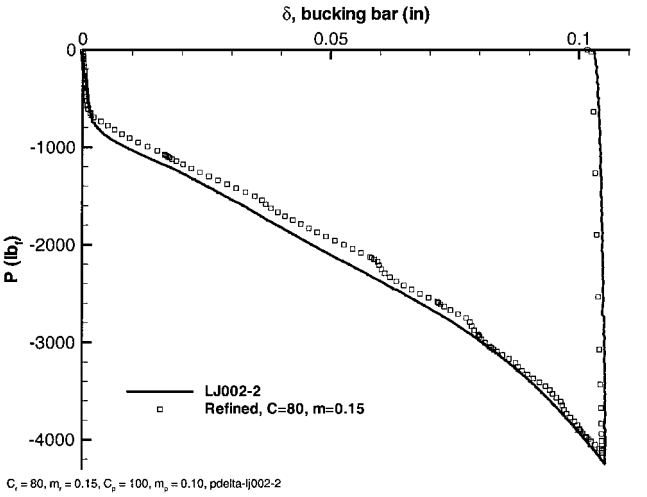

Fig. 8 Comparison between experimental and finite element force-deflection responses for the riveting bucking bar during the installation process with a squeeze force of 4250 lbf.

A photograph of a sectioned assembly with an overlay of a corresponding deformed finite element mesh is presented in Fig. 9, along with comparisons of measured and finite element values for several geometric characteristics of installed rivet configurations for two squeeze forces (Table 2).

The large difference between the finite element predictions and measured expansions of the hole should be interpreted carefully in light of the standard deviation of the hole diameters [600 μin.

Table 2 Comparison between finite element predictions and measurements of various geometric characteristics of installed rivets for two squeeze forces

Configuration	FEM	Exp.	Difference, %
	P = 3000 lb		
Expansion at *A*, in.	0.0002	0.001	−80
Expansion at *C*, in.	0.0015	0.002	−25
D_{max}, in.	0.2353	0.238	−1.1
H, in.	0.1202	0.124	−3.1
	P = 4000 lb		
Expansion at *A*, in.	0.005	0.009	−44
Expansion at *C*, in.	0.0042	0.005	−12.5
D_{max}, in.	0.2545	0.259	−1.7
H, in.	0.0999	0.101	−1.1

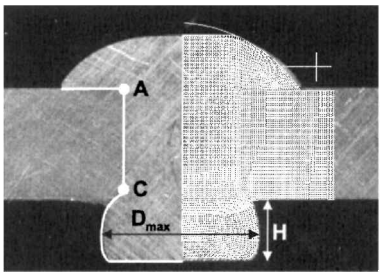

Fig. 9 Deformed finite element mesh superimposed over a polished section at and around an installed rivet/plate assembly. The dimensions referred to in Table 2 are defined in this figure.

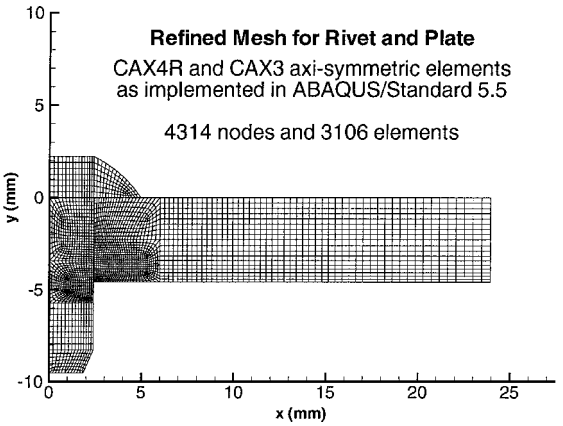

Fig. 10 Visualization of the axisymmetric refined mesh used in the finite element modeling of the rivet installation process.

(15 μm)] and accuracy of the optical measurement [approximately 750 μin. (20 μm)]. That is, as both the finite element and actual radial deformations along thickness of the hole are on the order of these sources of variability, the quoted difference value is highly sensitive to these factors. Note that the difference between the finite element and measured values for the large-scale deformations (maximum head diameter and head height) display a much better agreement with the model results.

Model Results

With a high degree of confidence in the model established, conclusions about the residual stress field induced by rivet installation and its potential impact on subsequent fatigue cracking can be made by interpreting the model results. For this purpose, a refined mesh (Fig. 10) was used to capture better the deformations and residual stresses near the area between both the driven head and plate edge and through the thickness of the hole. No appreciable difference in either the hole expansion values or force-deflection histories existed between the baseline and refined models, pointing toward numerical convergence of each model. Figures 11–13 present model results for a range of maximum squeeze forces (2500, 3500, and 4250 lbf). Included in Figs. 11–13 are contours of radial, tangential, and von Mises residual stresses; a profile of expansion of the hole edge through the thickness of the plate; and a deformed mesh after unloading, highlighting the configuration of the driven head.

In comparing the radial residual stresses σ_{11}, an indicator of the residual interference between the rivet and plate, two features stand out. First, as expected, the magnitude of the compressive residual stresses increases with squeeze force, with greater expansion of the rivet against the hole interface. Second, and more important, is the variation of the magnitude of the radial stresses (and hole expansion, as reflected in the results) through the thickness of the plates. Recall the earlier comment that most models of riveted joints account for only an artificially induced level of uniform through-thickness interference.

Similar conclusions can be drawn from the contours of tangential residual stress. Note that it is this hoop stress σ_{33} that can have a marked impact on the propagation of fatigue cracks that nucleate at either the edge of the rivet hole or the faying surfaces of the plates. As with the radial residual stresses, the contours of residual hoop stress exhibit both a variation in the thickness direction and a dependence on maximum squeeze force. Of particular interest is the zone of compressive residual stress at the edge of the hole near the driven head. At first, the compressive nature of this residual hoop stress might seem to conflict with the notion of hole expansion. The presence of this area of compressive hoop stress can be explained qualitatively, though, by looking at the yielding behavior of the material in the absence of stress in the thickness direction, σ_{22}. According to the Tresca criterion,

$$|\sigma_{11} - \sigma_{33}| \leq \sigma_y \tag{1}$$

As the rivet expands against the hole and the interfacial contact pressure exceeds the yield point of the material ($\sigma_{11} < -\sigma_y$), the material deforms in such a manner as to force $\sigma_{33} < 0$. Such a compressive residual hoop stress is often induced around rivet holes prior to riveting by cold working the hole with an expanding mandrel, with the goal of retarding the growth of fatigue damage that may nucleate in the material at and around the hole.

As displayed in the contours of the residual hoop stress, the size and magnitude of the compressive zone increases with increasing maximum squeeze force. In maintaining the compatibility of the material in the hoop direction, however, this compressive zone is balanced by an area of tensile stress away from the hole periphery. As exhibited in the contours, a region of tensile hoop stress is present beyond the compressive region in the lower sheet.

The location of this tensile zone becomes critical when considering the nucleation and subsequent propagation of fatigue cracks that nucleate not at the rivet/hole interface, but at the faying surface, away from the hole periphery. Note that an increasing maximum squeeze force not only pushes the zone of tensile stress away from the hole periphery, but also results in a larger driven head size. In spite of these large driven heads, none of the cases analyzed resulted in appreciable levels of residual clamping pressure through the thickness. This finding is contrary to that of Müller[2] for a slug-type rivet, with a driven head on both ends, but consistent to modeling results by Fawaz.[18]

Although the driven rivet head induces no inherent clamping pressure while the joint is unloaded, larger driven heads can provide increased clamping resistance as load is applied to the lap splice and localized out-of-plane deformation occurs in the vicinity of the rivet. Thus, from the earlier discussion of the dual-mode load transfer mechanism, larger driven heads produced by high squeeze forces would result in a larger percentage of load being transferred via friction at the faying surface. The resulting increased intensity in contact stresses at the interface also increases the potential for nucleation of fatigue damage away from the hole periphery, closer to the zone of tensile hoop stress. Thus, higher squeeze forces offer the ability to improve fatigue performance by retarding the growth of cracks from the hole edge, while increasing the potential for nucleation and accelerated propagation of faying surface fretting fatigue cracks.

Figure 14 solidifies a quantitative link between rivet process parameters and fatigue performance by presenting fatigue lifetimes

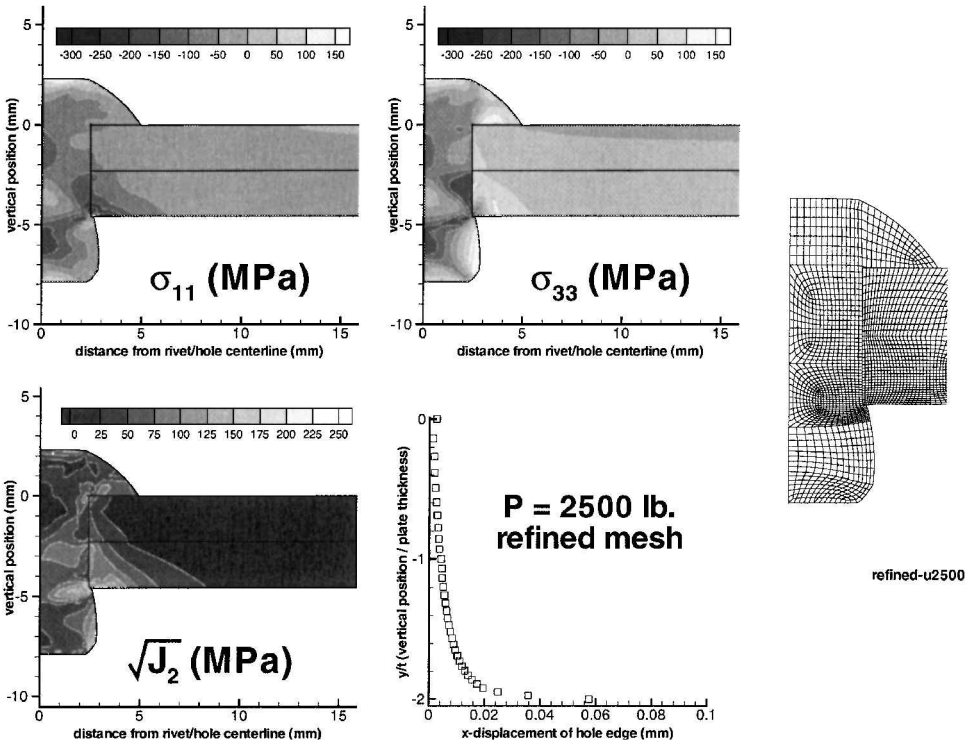

Fig. 11 Results from a finite element analysis with refined mesh for a maximum squeeze force of 2500 lbf.

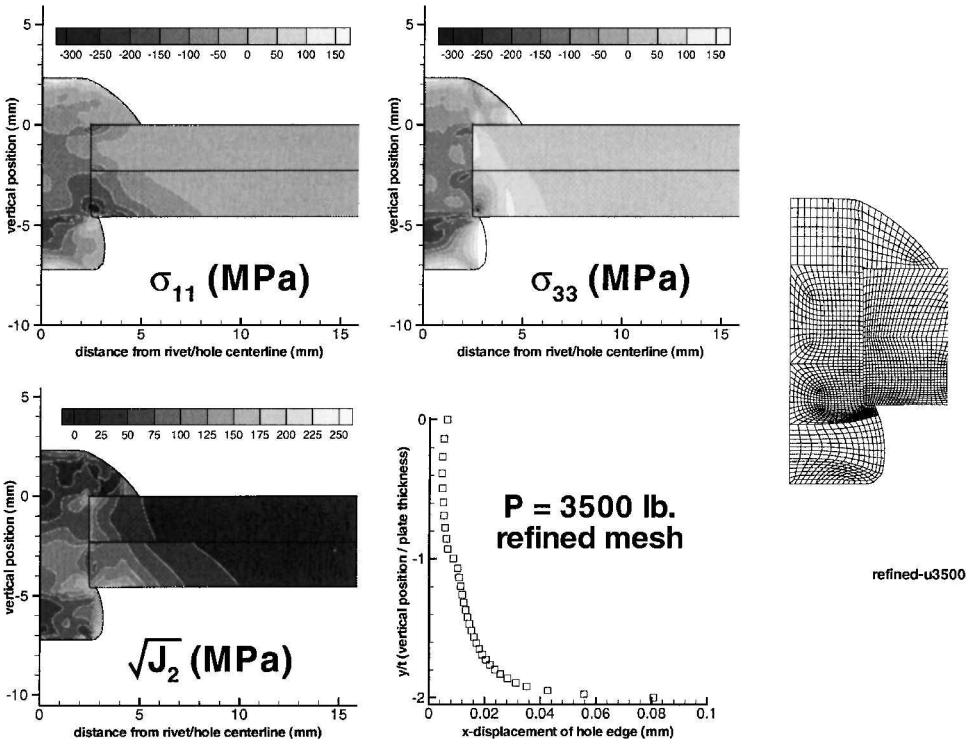

Fig. 12 Results from a finite element analysis with refined mesh for a maximum squeeze force of 3500 lbf.

of 12 single-lap joints manufactured with varied and controlled squeeze forces and tested to failure in a separate study.[4] As should be anticipated, fatigue life decreased with an increase in applied load. In addition, joint life increased with larger maximum squeeze forces. Whereas part of this difference in life must be attributed to the compressive residual stresses induced by the increased hole expansion associated with the higher squeeze force, a second potential source is revealed by comparing the nature of the faying surface damage reported by Szolwinski et al. in a summary of observations from the lap joint tests[4]: The joints manufactured with higher squeeze forces showed distinct signs of fretting wear debris on the faying surface near the rivet hole, whereas the faying surface of the joints riveted with lower forces exhibited no signs of such damage.

As conjectured earlier, this characteristic damage provides direct evidence of the impact that the riveting process parameters have on the load transfer mechanism in the joint: Larger driven heads

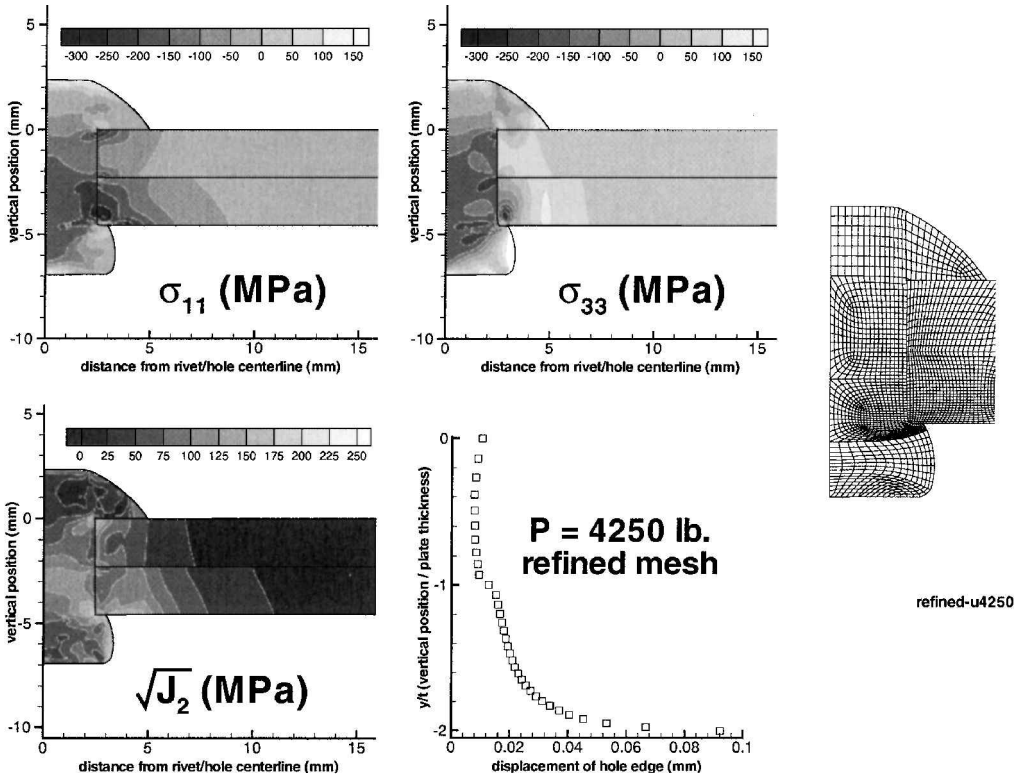

Fig. 13 Results from a finite element analysis with refined mesh for a maximum squeeze force of 4250 lbf.

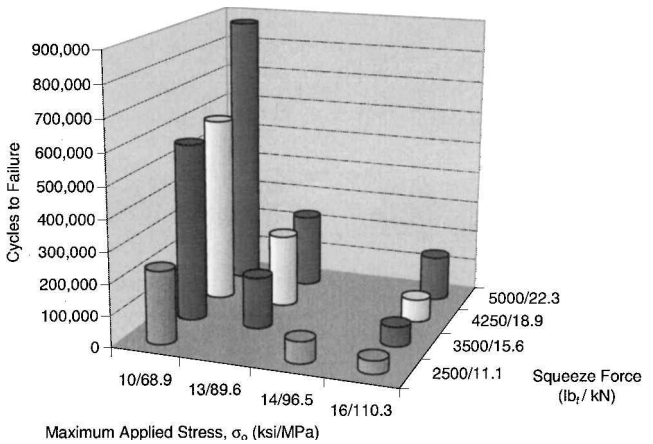

Fig. 14 Summary of single-lap joint fatigue tests results; observed cycles to failure for each test plotted against the riveting process parameter and applied bulk stress.

provide increased clamping constraint at the faying surface leading to an increased amount of frictional load transfer (and fretting fatigue damage) at this interface. Juxtaposing an assessment of these residual stresses with finite element models of single lap joint riveted structures have provided insight into the state of cyclic stress and strain responsible for the nucleation of fretting fatigue damage at and around the rivet/hole interface, an effort beyond the scope of this paper. This quantitative assessment of the localized conditions has been used successfully with a fatigue life parameter to predict the fatigue performance of riveted single-lap joint structures manufactured under controlled conditions.[4,19]

Conclusions

A finite element model of force-controlled rivet installation has been formulated in a commercially available analysis package and verified with a series of well-characterized experiments. Results from this analysis reveal a distinct through-thickness dependence of the residual stress field, contrary to assumptions prevalent in the literature and critical to understanding the nature of fatigue crack nucleation and propagation around the rivet/hole interface. Furthermore, the model has established a conclusive link between rivet process parameters and the nature of the resulting residual stresses. Of particular interest is the distribution of hoop stress associated with high squeeze forces (or increased hole expansion): A zone of compressive residual hoop stress dominates the area near the hole periphery, whereas a zone of tensile residual hoop stress pervades an area away from the hole. These zones of residual hoop stress can have a profound impact on the propagation of fatigue damage that nucleates at both the rivet/hole interface or faying surface.

Acknowledgment

This work was supported in part through a multidisciplinary University Research Initiative F49620-98-1-0293 from the U.S. Air Force Office of Scientific Research designed to address basic concerns facing the fleet of aging aircraft, both civilian and military.

References

[1] Piascik, R. S., and Willard, S. A., "The Characteristics of Fatigue Damage in the Fuselage Riveted Lap Splice Joint," NASA TP-97-206257, Nov. 1997.

[2] Müller, R. P. G., "An Experimental and Analytical Investigation on the Fatigue Behavior of Fuselage Riveted Lap Joints," Ph.D. Thesis, Delft Univ. of Technology, Delft, The Netherlands, Oct. 1995.

[3] Hoeppner, D. W., Elliott, C. B., III, and Moesser, M. W., "The Role of Fretting Fatigue on Aircraft Rivet Hole Cracking," TR DOT/FAA/AR-96/10, Dept. of Transportation, Federal Aviation Administration, Oct. 1996.

[4] Szolwinski, M. P., Harish, G., McVeigh, P. A., and Farris, T. N., "Experimental Study of Fretting Crack Nucleation in Aerospace Alloys with Emphasis on Life Prediction," *Fretting Fatigue: Current Technology and Practices*, ASTM STP 1367, edited by D. W. Hoeppner, V. Chandrasekaran, and C. B. Elliott, American Society for Testing and Materials, West Conshohocken, PA (to be published).

[5] Beuth, J. L., and Hutchinson, J. W., "Fracture Analysis of Multi-Site Cracking in Fuselage Lap Joints," *Computational Mechanics*, Vol. 13, No. 5, 1994, pp. 315–331.

[6] Park, J. H., and Atluri, S. N., "Fatigue Growth of Multiple-Cracks Near a Row of Fastener-Holes in a Fuselage Lap Joint," *Computational Mechanics*, Vol. 13, No. 3, 1993, pp. 189–203.

[7]Fung, C. P., and Smart, J., "An Experimental and Numerical Analysis of Riveted Single Lap Joints," *Journal of Aerospace Engineering*, Vol. 208, No. 2, 1994, pp. 79–90.

[8]Iyer, K. A., "Three-Dimensional Finite Element Analyses of the Local Mechanical Behavior of Riveted Lap Joints," Ph.D. Thesis, Materials Science and Engineering, Vanderbilt Univ., Nashville, TN, May 1997.

[9]Harish, G,. and Farris, T. N., "Shell Modeling of Fretting in Riveted Lapjoints," *AIAA Journal*, Vol. 36, No. 6, 1998, pp. 1087–1093.

[10]Hartman, A., "The Influence of Manufacturing Procedures on the Fatigue Life of 2024-T3 Alclad Riveted Single Lap Joints," National Lucht-En Ruimtevaartlaboratorium, TR NLR TR 68072 U, Amsterdam, July 1968.

[11]Donaldson, D. R., and Kenworthy, K. J., "Fatigue Design and Test Program for the American SST," *Aircraft Fatigue Design, Operational and Economic Aspects*, edited by J. Y. Mann and I. S. Milligan, Pergamon, Rushcutters Bay, 1972, pp. 437–476.

[12]Szolwinski, M. P., "The Mechanics and Tribology of Fretting Fatigue with Application to Riveted Lap Joints," Ph.D. Thesis, School of Aeronautics and Astronautics, Purdue Univ., West Lafayette, IN, 1998.

[13]"ABAQUS/Standard 5.5 User's Manual," Vol. 1, Hibbitt, Karlsson, and Sorensen, Inc., Pawtucket, RI, 1997, Section 6.1.2, p. 2.

[14]*Metallic Material and Elements for Aerospace Vehicle Structures*, MIL-HDBK-5G, Vol. 1, Defense Printing Service Detachment Office, Philadelphia, PA, 1994.

[15]*ASM Metals Handbook, Desk Edition*, American Society for Metals, Metals Park, OH, April 1997.

[16]Thomsen, E. G., Yang, C. T., and Kobayashi, S., *Mechanics of Plastic Deformation in Metal Processing*, MacMillan, New York, 1965.

[17]Reithmaier, L., *Standard Aircraft Handbook*, Tab AERO, Blue Ridge Summit, PA, 5th ed., 1991.

[18]Fawaz, S. A., "Fatigue Crack Growth in Riveted Joints," Ph.D. Thesis, Delft Univ., Delft, The Netherlands, 1997.

[19]Harish, G., and Farris, T. N., "An Integrated Approach for the Prediction of Fretting Crack Nucleation in Riveted Lap Joints," AIAA Paper 99-1340, April 1999.